Taiming Luo, Jianwei Wei*, Xiaozhan Yang, Daoyuan Wang and Wenlin Feng*

Trace Hydrogen Sulphide Gas Sensor Based on Cu/rGO Membrane-Coated Photonic Crystal Fibre Michelson Interferometer

https://doi.org/10.1515/zna-2019-0341 Received November 20, 2019; accepted February 5, 2020; previously published online March 7, 2020

Abstract: A novel Michelson interferometric hydrogen sulphide sensor coated with copper/reduced graphene oxide (Cu/rGO) composite membrane is proposed and fabricated. A section of endlessly photonic crystal fibre (EPCF) was sandwiched in two single-mode fibres (SMFs). One SMF was spliced and tapered with EPCF; the other SMF was connected with the Faraday rotator mirror to construct the Michelson structure. The cladding of the EPCF was coated by the Cu/rGO-sensing membrane, which was prepared by the dip-coating method. The obtained Cu/rGOsensing film has a length of 25.0 mm. The fabricated sensing membrane is characterised by the scanning electron microscopy, X-ray photoelectron spectroscopy (XPS), Raman spectroscopy, and so on. Experimental results demonstrated that the Cu/rGO-sensing film has a 24.56nm thickness with a compact and uniform appearance. The XPS and Raman spectra indicate that there are three elements (C, O, and Cu), which are consistent with the expected compositions of the Cu/rGO membrane. With the increase of concentration of hydrogen sulphide, the interference spectra appear red-shifted. The linearity of 0.97662 and the sensitivity of 13.23 pm/ppm are achieved. In addition, the dynamic response and recovery time of the sensor

*Corresponding authors: Jianwei Wei and Wenlin Feng,

Department of Physics and Energy, Chongqing University of Technology, Chongqing 400054, PR China; and Chongqing Key Laboratory of Modern Photoelectric Detection Technology and Instrument, Chongqing 400054, PR China, Tel.: +86 23 6256 3055, E-mail: redskywei@cqut.edu.cn (J. Wei); wenlinfeng@126.com (W. Feng)

Taiming Luo: Department of Physics and Energy, Chongqing University of Technology, Chongqing 400054, PR China. https://orcid.org/0000-0003-0645-7653

Xiaozhan Yang: Department of Physics and Energy, Chongqing University of Technology, Chongqing 400054, PR China; and Chongqing Key Laboratory of Modern Photoelectric Detection Technology and Instrument, Chongqing 400054, PR China Daoyuan Wang: Department of Chemistry and Physics, University of Arkansas at Pine Bluff, Pine Bluff, AR 71601, USA

are approximately 70 and 88 s, respectively. The surface adsorption energies of the film are calculated by the density functional theory. The theoretical results are in good agreement with the experimental findings. This sensor has some key advantages of small size, simple structure, easy fabrication, and great applicability for detecting the trace hydrogen sulphide.

Keywords: Gas Sensor; Michelson Interferometer; Photonic Crystal Fibre; Reduced Graphene Oxide; Sensing Membrane.

1 Introduction

Hydrogen sulphide (H₂S) is a colorless, flammable, odorous, and toxic gas. The natural lipolysis of hydrogen sulphide brings it to be absorbed by human lung and blood and damages human organs [1, 2]. It often exists in sewers, reservoirs, petrochemical factories, heavy water production, agriculture, and hot springs, which often cause the incidents of hydrogen sulphide poisoning [3, 4]. At present, H2S detections are commonly used by the metal oxide semiconductor sensors, solid electrolyte sensors, polymer electrolyte sensors, and heater resistance sensors [5-7]. However, it is still unfavourable in the performance of selectivity, stability, and antielectromagnetic interference [8–15], whereas the optical fibre sensors can overcome the above problems [16]. Among them, the fibreoptic Michelson interferometric sensor has the advantages of strong selectivity, good stability, high sensitivity, antielectromagnetic interference, small size, low cost, simple structure, and so on. At the same time, this kind of sensor can be applied in gas detection, temperature, pressure, strain measurement, and filter modulation [17-20]. In gas detection, the performance of sensing film is very important because the surface interaction between gas and membrane demands good efficiency. It is found that the nano-copper/reducing graphene oxide (rGO) composite film can enhance the photostability and photocurrent density when compared to that of only the rGO membrane [21]. The addition of copper appears to increase the adsorption abilities and efficiencies between the gas

molecules and those hydroxyl groups that are distributed on the surface of rGO [22, 23]. But so far, the optical fibre Michelson gas sensor combined with the Cu/rGO film has not been reported yet in the previous literatures.

In this work, a Michelson interferometric hydrogen sulphide sensor coated with Cu/rGO-sensing film is proposed and constructed. Two standard single-mode fibres (SMFs) were spliced at both ends of an endlessly photonic crystal fibre (EPCF) to form the SMF-EPCF-SMF structure. One end of the structure is tapered, and the other end of the sensor is connected with a fibre-optic Faraday rotator mirror (FRM). The surface of EPCF is coated with a Cu/rGO-sensing film. Finally, the multibeam interference is formed in the tapered region. In addition, because of the reflection of the FRM, the interference is strengthened, and the contrast of interference fringe is improved, which effectively increases the sensitivity of the sensor. At the same time, the density functional theoretical calculation is used in the selectivity analysis. The results are discussed.

2 Principle

The single tapered Michelson interferometric hydrogen sulphide sensor coated with Cu/rGO-sensing film is shown in Figure 1. The tapered structure of optical fibre has been extensively studied as power couplers and splitters [24–26]. The cladding and the core lights are reflected by the reflector and coupled back to the core in the tapered region. The phase difference $(\Delta \varphi)$ between cladding and core modes can be given as follows:

$$\Delta \varphi = 4\pi (n_{\text{cladding}} - n_{\text{core}}) L/\lambda = 4\pi \Delta n_{\text{eff}} L/\lambda$$
 (1)

where $n_{\rm cladding}$ and $n_{\rm core}$ are the refractive indices of the cladding and core, respectively. $\Delta n_{\rm eff}$ is the difference between $n_{\rm cladding}$ and $n_{\rm core}$. L is the length of the sensing region, and λ is the wavelength of the incident light.

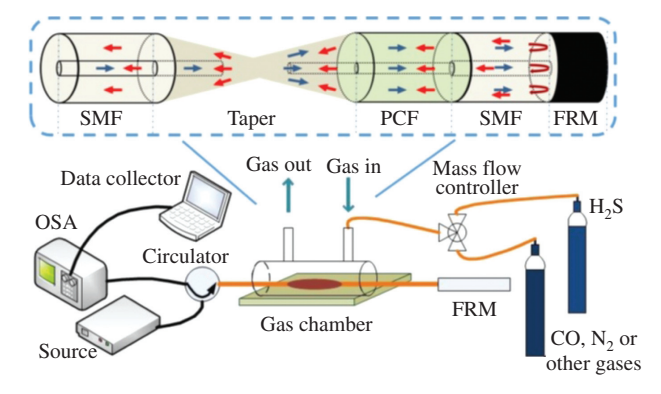


Figure 1: Schematic diagram of the experimental setup. The inset shows the fibre-optic Michelson structure.

According to the phase relation of Michelson interference enhancement and attenuation, the condition of maximum interference attenuation can be expressed as follows:

$$\Delta \varphi = (2k+1)\pi \tag{2}$$

where k can be any integer.

Combining (1) and (2), the following formula can be given as

$$\Delta \lambda = 4\Delta n_{\rm eff} L/(2k+1) \tag{3}$$

Obviously, the wavelength shift $(\Delta\lambda)$ is proportional to refractive index difference $(\Delta n_{\rm eff})$. Because of the constancy of the $n_{\rm core}$, the $\Delta n_{\rm eff}$ will change with various $n_{\rm cladding}$. When the sensing film adsorbs gas molecules, the tiny change of the cladding refractive index will lead to the movement of the monitoring trough [27]. Therefore, by monitoring the variation of the trough, the gas concentration information can be obtained accordingly.

3 Experiment and Methods

3.1 Sensor Fabrication

The standard SMF and EPCF fibres were bought from Yangtze Optical Fibre and Cable Joint Stock Limited Company (YOFC, Wuhan, China). The cladding diameter of EPCF is 125 µm, with multilayer air holes of 9.5 µm in diameter, arranged in a hexagonal structure with a length of 31.5 mm. The optical fibre fusion machine is S178C type, Furukawa, Japan. The light source is ASE broadband light source (Kangguan, Beijing, China). The annulus is PIOC315P210 type (Xianlian Co., Ltd., Sichuan, China), and the spectrum analyser is used by AQ6370D spectrometer (Yokogawa, Tokyo, Japan). In the preparation process of sensing structure, the manual splicing procedure is adopted, and the parameters are set in Table 1. At this time, the ends between SMF and EPCF are spliced to form a shrunk taper, and the other end of EPCF is spliced with another SMF and connected with an FRM. Thus, the Michelson interferometer is obtained and illustrated in the inset of Figure 1.

3.2 Preparation and Characterisation of Sensing Membrane

The 3.2 g/L nano-copper with diameter of 5–10 nm and GO aqueous dispersion solutions were bought from Nanjing Xianfeng Nano Material Technology Co., Ltd., Nanjing, China. The Cu/rGO-sensing film is prepared by the dip-coating method. First, 500 μL graphene oxide (GO) aqueous dispersion solution is mixed in 300 μL isopropanol and 200 μL 30 % hydrogen peroxide solution and then dispersed uniformly by ultrasound for 20 min to obtain GO mixed solution. Second, 700 μL nano-copper aqueous dispersion is added to 300 μL isopropanol for ultrasonic dispersion. The EPCF is, respectively immersed in GO and nano-copper solution for 10 min, and then it is dried by the vacuum freeze dryer, and the above dip-coating

Table 1: The procedures and setting parameters of the tapered fibre.

| Procedure | Parameter | Procedure | Parameter | |
|-------------------------------|----------------------|------------------------------|------------------|--|
| The first arc-power | +100 | Automatic discharge time | +1500 ms | |
| The first end arc-power | +100 | End time of first discharge | $+0~\mathrm{ms}$ | |
| The second arc-power | +40 | End time of redischarge | $+0~\mathrm{ms}$ | |
| The second end arc-power | +40 | Discharge compensation value | -20 | |
| The cleaning duration time | +200 ms | Clean discharge deviation | +20 | |
| The prefusion time | +160 ms | Discharge centre offset | −50 µm | |
| The initial arc-duration time | $+1000\;\mathrm{ms}$ | Z-pull distance | 15 μm | |
| The second arc-duration time | +2000 ms | Z-push distance | 400 μm | |

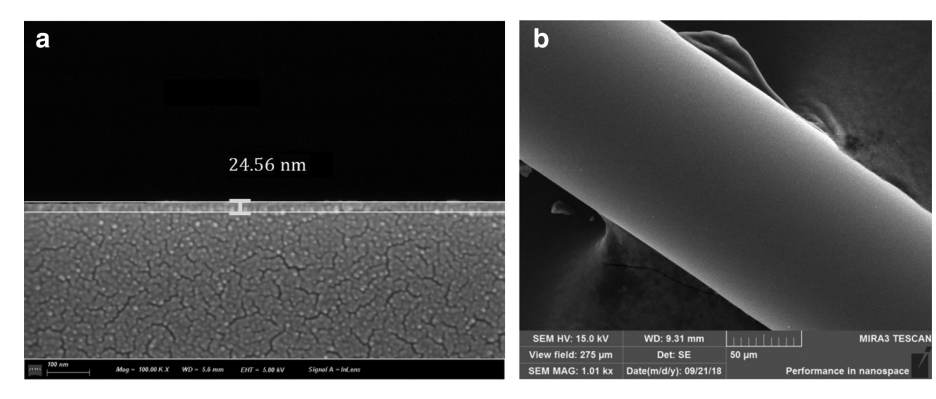


Figure 2: The SEM morphology of sensing film: (a) SEM image of the thickness of cross section and (b) SEM image of the side surface.

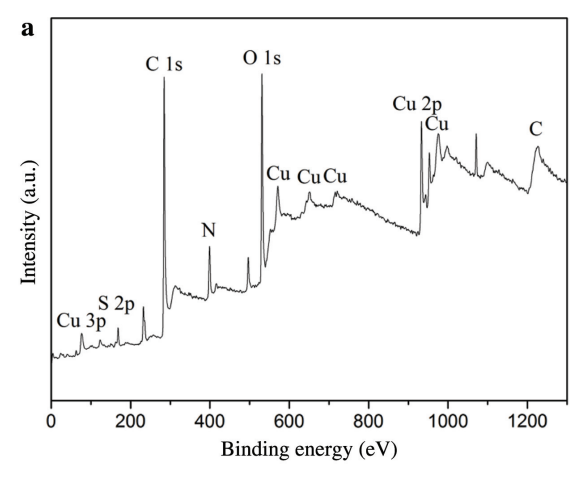
process is repeated alternately. Lastly, the coated fibre is placed in a tubular furnace, which is accessed by nitrogen and calcined at 300 °C for 2 h, and then the Cu/rGO membrane-coated EPCF is obtained. The scanning electron microscopy (SEM) results (Fig. 2) show that the film thickness is about 24.56 nm, and the film surface is dense and smooth. To further determine the element composition of the sensing film, X-ray photoelectron spectroscopy (XPS) and Raman spectroscopy are used.

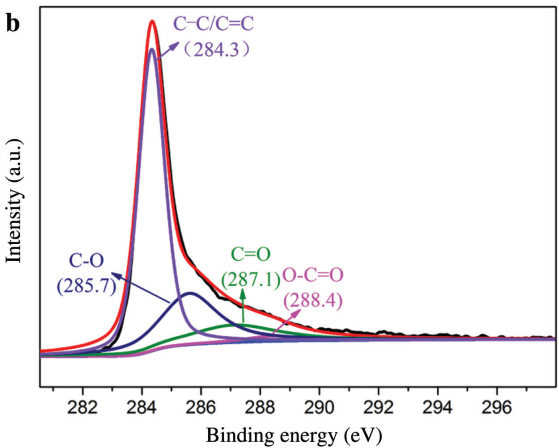
Figure 3 is the XPS of Cu/rGO composite membrane. Figure 3a is the full spectrum scanning of elements in the composite. The composite mainly contains three elements: C, O, and Cu. Figure 3b is a narrowband scan image of C1s after peak splitting. The binding energies corresponding to C-C/C=C, C-O, C=O, and O-C=O are 284.3, 285.7, 287.1, and 288.4 eV, respectively. Figure 3c is a narrowband scanning image of Cu2p after peak splitting. The binding energies of copper Cu⁺ 2P3/2, Cu²⁺ 2P3/2, Cu⁺ 2P1/2, and CuO 2P1/2 are 932.6, 934.6, 952.4/954.1, and 963 eV, respectively. These are in good agreement with the XPS results of the known Cu/rGO composites [21, 28-30]. It can be seen that nano-coppers are partially oxidised to CuO. In addition, the photoionisation cross section of H element has a low content, and the signal is too weak. Thus, the energy spectrum of H element cannot be displayed in XPS. Figure 4 is the Raman spectrum of the membrane. The intensity ratio of D to G peak is 1.053, which is consistent with the Raman peaks reported in literature [26], proving that GO is reduced to rGO.

3.3 Gas-Sensing Properties

Figure 1 is a schematic diagram of a single tapered Michelson interferometric hydrogen sulphide sensor based on the Cu/rGO-sensing film. H₂S gases 0-70 ppm are introduced into the gas chamber. Ambient air is used here in this experiment for gas dilution. The interference spectra obtained are shown in Figure 5. In the range of 0-70 ppm H₂S gas concentration, the interference spectra of the sensor show a significant red shift with the increase of H₂S gas concentration. The reason is that when the H₂S gas molecules contact with Cu/rGOsensing film, the refractive index of the film will increase because of the adsorption of H₂S gas. It can be seen from formula (3) that the interference spectra of the sensor will be red-shifted with the increase of H₂S gas concentration. The experimental results are in good agreement with the theoretical analysis. By fitting the spectral offset, the relationship between the spectral offset and the measured gas concentration is obtained. The linearity of the sensor is 0.97662, and the sensitivity is 13.23 pm/ppm. The limit of detection (LOD) of the gas sensor can be obtained according to the formula in literature [31, 32], that is, LOD = $3\sigma/K$, in which σ (0.000723 nm) is the standard deviation for the wavelength of the sensing system in the absence of H₂S, and K (0.01323 nm/ppm) denotes the slope of the fitting curve; thus, the low LOD (0.164 ppm) of this sensor is achieved. It is worth noting that the film with different thicknesses will all cause the interference spectra to shift to various extents. For a determined film thickness, the sensor's gas detection ability will not be affected because the reference valley wavelength is a determined and fixed value, which will not change during the measurements.

Figure 6 shows the response-recovery time curve of the sensor. The response time t_r and recovery time t_f of the sensor are approximately 70 and 88 s, respectively. Figure 7 shows the gas selectivity of the sensor. Compared with the same concentration of carbon monoxide, carbon dioxide, hydrogen, nitrogen, ammonia, and oxygen, the sensor has a high selectivity for hydrogen sulphide. The main reason is because hydrogen sulphide gas molecule is polar molecule. Compared to nonpolar molecules, such as carbon dioxide, nitrogen,





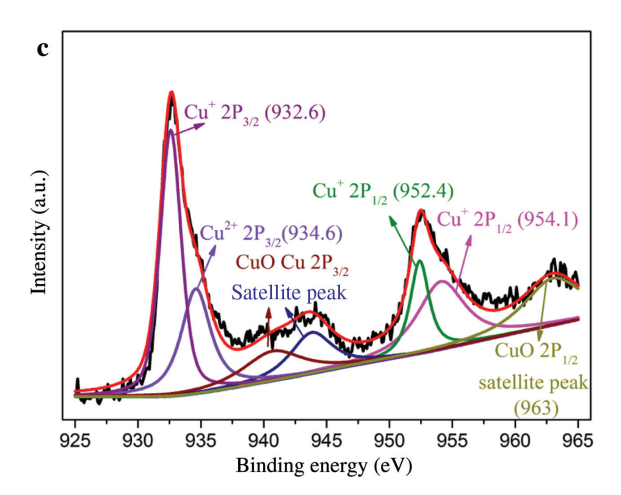


Figure 3: (a) XPS image of CuO/rGO membrane and the corresponding high-resolution XPS scans of (b) C 1s and (c) Cu 2p.

and oxygen, this Cu/rGO-sensing film results in a better adsorption on H_2S molecules. In addition, hydrogen sulphide is a reducing gas, which is easy to lose electron. There is a very weak chemisorption between the hydrogen sulphide gas molecule and nano-copper. Electrons obtained by copper ions (Cu²+ or Cu+) correspond to the response process of the gas sensor. On the contrary, it corresponds to the recovery process of the gas sensor. The relevant process formula is as follows: $Cu^+ \xrightarrow{\begin{subarray}{c} +e \end{subarray}} Cu$ or $Cu^{2+} \xrightarrow{\begin{subarray}{c} +e \end{subarray}} Cu^+$. At the same

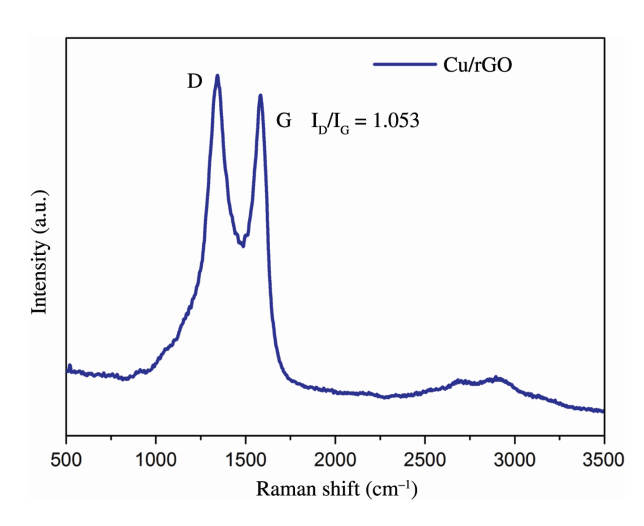


Figure 4: Raman spectrum of Cu/rGO membrane.

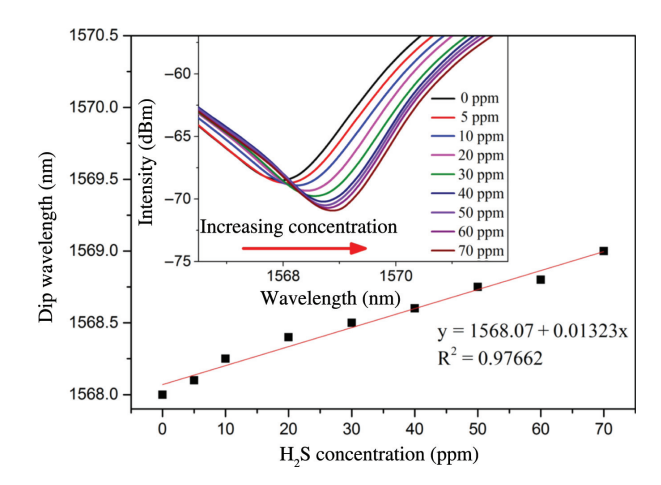


Figure 5: The wavelength shift upon the concentration of hydrogen sulphide. The inset shows the reflectance spectra of the sensor in various concentrations of hydrogen sulphide.

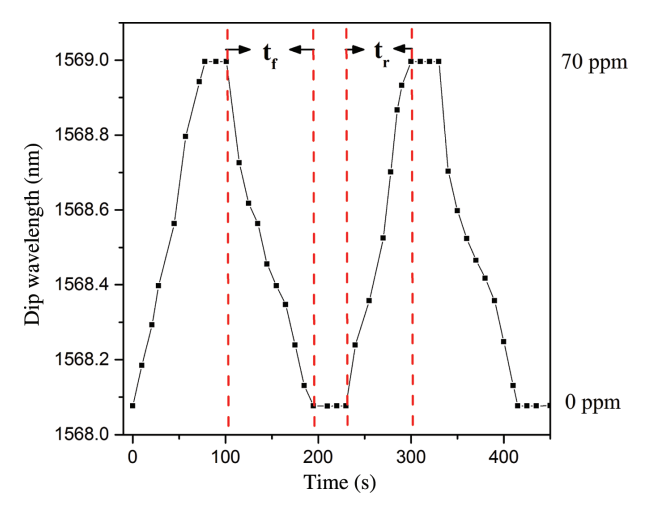


Figure 6: Dynamic response of the hydrogen sulphide sensor.

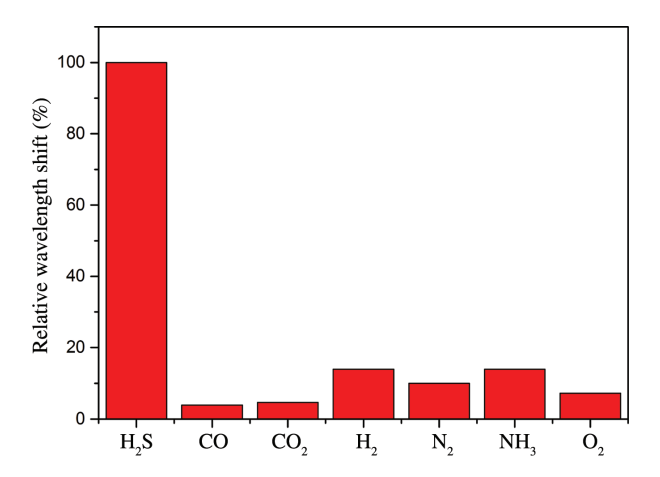


Figure 7: Selectivities for hydrogen sulphide, carbon monoxide, carbon dioxide, hydrogen, nitrogen, ammonia, and oxygen.

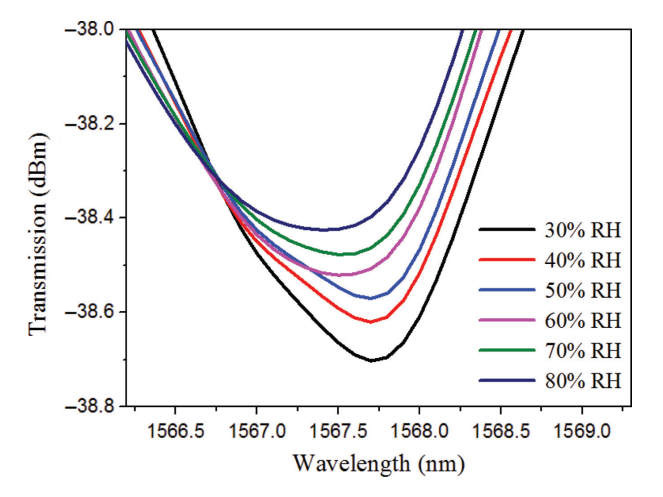


Figure 8: The interference valley wavelength shift dependence with various relative humidity (monitoring at 300 K).

time, H_2S has the maximum molecular radius among the above gas molecules; the binding capacity of the outermost electrons on the 3P orbital is weak and easy to give electrons to the sensing film. Thus, the sensor has a high selectivity for hydrogen sulphide gas. Among these molecules, except hydrogen sulphide, the selectivity of H_2 and NH_3 is relatively slightly higher than those of other gases, mainly because the rGO has a certain hydrogen adsorption capacity [33]. Ammonia is a polar molecule. It can be attracted/absorbed to the polar functional groups that are located on the surface of rGO. Although these adsorptions are weaker than those of other chemical bondings, they are still much stronger than physical adsorption. It is worth noting that CO's polarity is weak because of the π backbonding. Therefore, the selectivity of CO is poor.

The sensor's response to moisture has been performed by the experiment. Figure 8 is the interference valley wavelength shift dependence on various relative humidity levels (monitoring at 300 K). With the increase of relative humidity, the spectral interference valley shows a blue shift. When the relative humidity is 80 %, the interference valley wavelength moves 0.32 nm, compared to that of 30 % humidity. When the relative humidity increases from 30 % to 50 %, the interference valley wavelength moves 0.06 nm.

However, the relative humidity increased from 50 % to 80 %; the interference valley wavelength is shifted 0.26 nm. Therefore, in the relative humidity range of 30 %–50 %, the sensor is less affected by the moisture. Therefore, the sensor has certain application value when the relative humidity is lower than 50 %.

4 Theoretical Calculation

The adsorption energies of several typical gases (H_2S , CO, CO_2 , H_2 , N_2 , NH_3 , and O_2) were calculated by the density functional theory. For Cu/rGO, the lattice consists of 62 carbon atoms, 4 oxygen atoms, 1 copper atom, and 3 hydrogen atoms. The existence of hydrogen atoms is due to a very small amount of hydrogen functional groups on the surface of rGO. The molecular structures and total energy are calculated by the density functional simulation software SIESTA [34]. The relaxation atomic force is less than 0.02 eV/Å. The used pseudopotential is a generalised gradient approximation pseudopotential modified by PBE (Perdew–Burke–Ernzerhof) [35].

In order to minimize the error, the double- ζ polarisation basis set is used to express the wave function of the valence electrons. The calculation of the gas adsorption energy is based on the same Cu/rGO lattice, and the total energy is calculated at 300 K and 300-Ry cutoff energy [35]. The adsorption sites are shown in Figure 9, and the gas adsorption structures and their corresponding energies at different adsorption sites are given in Table 2. The average adsorption energies follow the order of H₂S > $H_2 > NH_3 > N_2 > O_2 > CO_2 > CO$, which is also consistent with the order of gas selectivity in Figure 7. Therefore, among the seven gases, rGO has a high adsorption capacity for hydrogen sulphide; the addition of copper has a catalytic action on the adsorption of hydrogen sulphide. Reducing graphene oxide strongly attracts hydrogen in hydrogen sulphide because hydrogen atom in hydrogen sulphide is relatively positively charged, whereas carbon atoms in rGO are relatively negatively charged; electrostatic attraction also occurs between them. According to the order of adsorption energy, it can be considered that an extremely weak chemical adsorption appears at 300 K, which is the process of adsorption and desorption of hydrogen sulphide. For other gases, physical adsorption can be considered, as shown in Figures 7 and 9.

The comparisons (sensor type, detection limit, working temperature, response time t_r , and recovery time t_f) of several H₂S detection methods between this work and other studies are shown in Table 3 [36–39]. Compared with the heterostructural tubule heater and chemiresistor gas sensor, fibre gas sensor can work without electricity at room temperature and has a higher

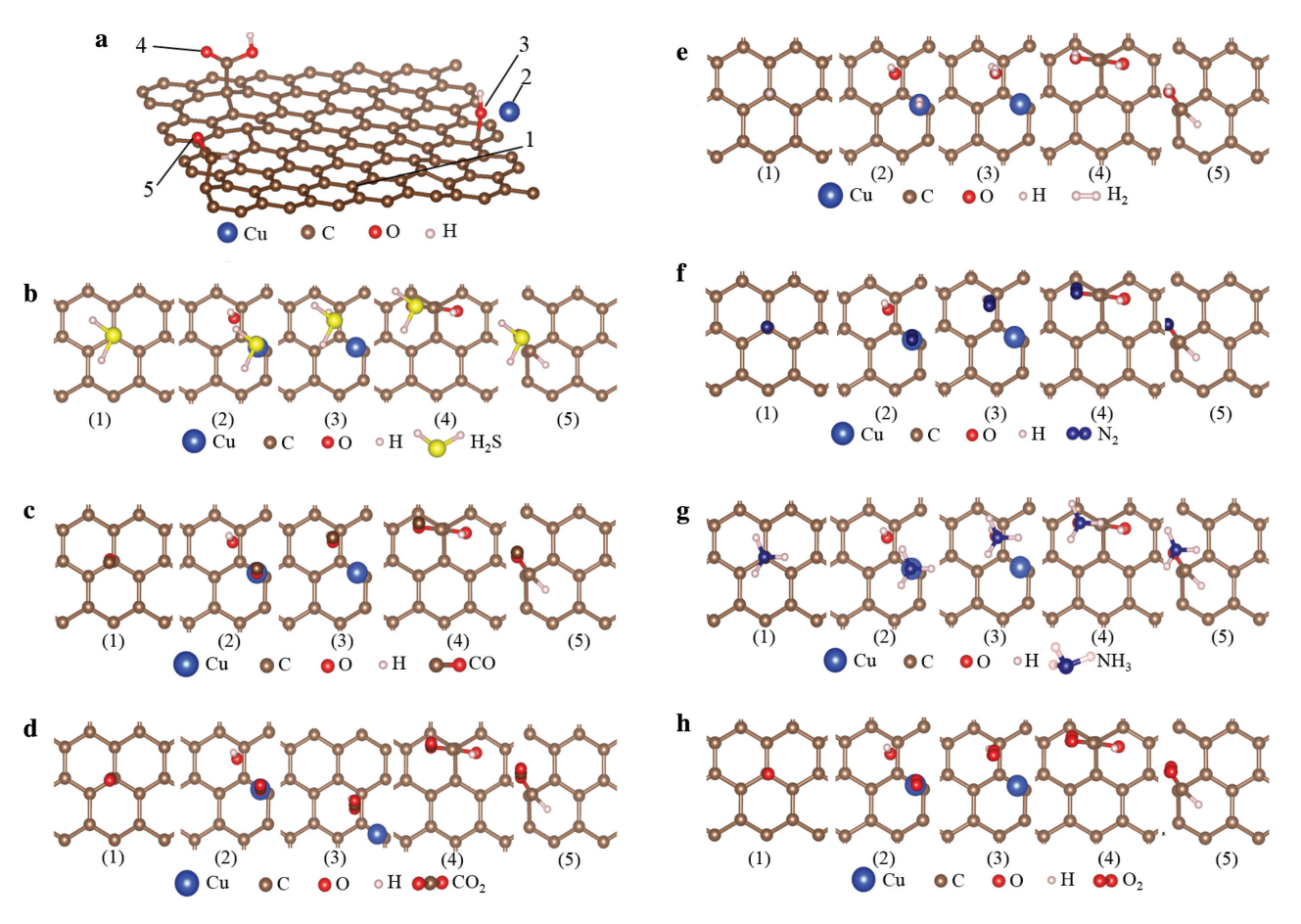


Figure 9: (a) The adsorption sites of the rGO. Adsorption structures of (b) hydrogen sulphide, (c) carbon monoxide, (d) carbon dioxide, (e) hydrogen, (f) nitrogen, (g) ammonia, and (h) oxygen.

Table 2: The average adsorption energies of different gases and the adsorption energies of the different sites (all the units are eV).

| Gases | 1 | 2 | 3 | 4 | 5 | Average |
|------------------|-----------|-----------|-----------|-----------|-----------|------------|
| Sites | | | | | | |
| H ₂ S | -0.099274 | -0.122494 | -0.095402 | -0.090620 | -0.091545 | -0.0998670 |
| CO | -0.001350 | -0.001303 | -0.000995 | -0.000610 | -0.000605 | -0.0009730 |
| CO_2 | -0.007686 | -0.007653 | -0.009182 | -0.005671 | -0.007722 | -0.0075832 |
| H ₂ | -0.054136 | -0.073801 | -0.066748 | -0.078403 | -0.062966 | -0.0672108 |
| N_2 | -0.016218 | -0.018953 | -0.018464 | -0.015561 | -0.019579 | -0.0177553 |
| NH_3 | -0.092806 | -0.063407 | -0.061889 | -0.009136 | -0.062862 | -0.0500200 |
| O_2 | -0.011654 | -0.013172 | -0.014742 | -0.010204 | -0.018331 | -0.0136209 |

Table 3: Comparisons (sensor type, detection limit, working temperature, response time t_r , and recovery time t_f) of several H₂S detection methods: long-period fibre grating (LPFG), heterostructural tubule (HT), electroactive polyimide (EP), optical fibre evanescent-wave sensing (OFEWS), and photonic crystal fibre Michelson interferometer (PCFMI).

| Sensor type | Detection limit (ppm) | Temperature (K) | t_r/t_f (s) | Reference | |
|-------------|-----------------------|-----------------|---------------|-------------------|--|
| LPFG | 0.5 | 300 | 89/97 | Qin et al. [36] | |
| HT | 0.01 | 443 | 35/29 | Na et al. [37] | |
| EP | 0.142 | 300 | 43/99 | Padua et al. [38] | |
| OFEWS | 5.1 | 300 | 2.03/- | Ke et al. [39] | |
| PCFMI | 0.164 | 300 | 70/88 | This work | |

chemical stability [36–39]. Therefore, fibre gas sensors including the fibre Michelson interferometer have a good safety application for the monitoring of nonelectric gas environment.

5 Conclusions

In this work, a single tapered Michelson interferometric hydrogen sulphide sensor based on the Cu/rGO-sensing film is proposed. The gas-sensing performance of the sensor is evaluated, and the results show that with the increase of H₂S concentration the central wavelength of its transmission spectrum shows red shift. The sensitivity of the sensor is 13.23 pm/ppm in the range of 0-70 ppm H_2S gas concentration. It has a good linearity and selectivity. The theoretical simulation results are consistent with the experimental findings. The sensor has the advantages of small size, light weight, easy preparation, high sensitivity, and selectivity. It has a potential application for trace H₂S gas detection in toxic environments.

Acknowledgements: This work was supported by the National Natural Science Foundation of China (Funder http://dx.doi.org/10.13039/501100001809, no. 51574054), the University Innovation Team Building Program of Chongging (grant no. CXTDX201601030), Scientific and Technological Research Program of Chongqing Municipal Education Commission (grant no. KJZD-M201901102), the Livelihood Project of Chongqing Science and Technology Bureau (grant no. cstc2017shmsA20017), and the Innovation Leader Project of Chongqing Science and Technology Bureau (grant no. CSTCCXLJRC 201905).

References

- [1] R. O. Beauchamp, J. S. Bus, J. A. Popp, C. J. Boreiko, et al., CRC Crit. Rev. Toxicol. 13, 25 (1984).
- [2] A. F. Abu-Hani, S. T. Mahmoud, F. Awwad, and A. I. Ayesh, Sens. Actuators B Chem. 241, 1179 (2017).
- [3] H. Daldal, B. Beder, S. Serin, and H. Sungurtekin, Clin. Toxicol. 48, 755 (2010).
- [4] D. H. Truong, M. A. Eghbal, W. Hindmarsh, S. H. Roth, and P. J. O'Brien, Drug Metabol. Rev. 38, 733 (2006).
- [5] A. Mirzaei, S. S. Kim, and H. W. Kim, J. Hazard. Mater. 357, 314 (2018).
- [6] X. Yang, Y. Zhang, X. Hao, Y. Song, X. Liang, et al., Sens. Actuators B Chem. 273, 635 (2018).
- [7] F. I. Ali, F. Awwad, Y. E. Greish, and S. T. Mahmoud, IEEE Sens. J. 19, 2394 (2018).

- [8] T. Hyodo, M. Takamori, T. Goto, T. Ueda, and Y. Shimizu, Sens. Actuators B Chem. 287, 42 (2019).
- H. Takeo, T. Yamashita, and Y. Shimizu, Sens. Actuators B [9] Chem. 207, 105 (2015).
- [10] A. Chowdhuri, V. Gupta, K. Sreenivas, R. Kumar, S. Mozumdar, et al., Appl. Phys. Lett. 84, 1180 (2004).
- [11] A. Ebrahimi, A. Pirouz, Y. Abdi, S. Azimi, and S. Mohajerzadeh, Sens. Actuators B Chem. 173, 802 (2012).
- [12] V. D. Kapse, S. A. Ghosh, G. N. Chaudhari, and F. C. Raghuwanshi, Talanta 76, 610 (2008).
- [13] M. Kaur, N. S. Ramgir, U. K. Gautam, S. K. Ganapathi, S. Datta, et al., Mater. Chem. Phys. 147, 707 (2014).
- [14] J. Kim and K. Yong, J. Phys. Chem. C 115, 7218 (2011).
- [15] M. MalekAlaie, M. Jahangiri, A. M. Rashidi, A. HaghighiAsl, and N. Izadi, Mater. Sci. Semiconduct. Proc. 38, 93 (2015).
- [16] R. Chen, W. Liu, G. Huang, D. Wang, X. Qin, et al., Appl. Opt. **57**, 9755 (2018).
- [17] A. D. Kersey, Int. Soc. Opt. Photonics 1367, 2 (1991).
- [18] B. H. Lee, Y. H. Kim, K. S. Park, J. B. Eom, M. J. Kim, et al., Sensors 12, 2467 (2012).
- [19] J. T. Zhou, Y. P. Wang, C. R. Liao, B. Sun, J. He, et al., Sens. Actuators B Chem. 208, 315 (2015).
- [20] T. Zhu, D. Wu, M. Liu, and D. W. Duan, Sensors 12, 10430 (2012).
- [21] X. Q. An, K. F. Li, and J. W. Tang, ChemSusChem 7, 1086 (2014).
- [22] L. N. Sun, Q. W. Deng, Y. L. Li, L. B. Deng, Y. Y. Wang, et al., Electrochim. Acta 222, 1650 (2016).
- [23] B. Elyassi, Y. Al. Wahedi, N. Rajabbeigi, P. Kumar, J. Seok, et al., Micropor. Mesopor. Mat. 190, 152 (2014).
- [24] J. D. Love, W. M. Henry, W. J. Stewart, R. J. Black, S. Lacroix, et al., IEE Proc. J. (Optoelectronics) 138, 343 (1991).
- [25] Y. He and F. G. Shi, Opt. Commun. 260, 127 (2006).
- [26] Z. Tian, S. S. Yam, and H. P. Loock, Opt. Lett. 33, 1105 (2008).
- [27] R. Jha, J. Villatoro, G. Badenes, and V. Pruneri, Opt. Lett. 34, 617 (2009).
- [28] J. Choi, H. Oh, S. W. Han, S. Ahn, J. Noh, et al., Curr. Appl. Phys. 17, 137 (2017).
- [29] V. V. Nikesh, A. B. Mandale, K. R. Patil, and S. Mahamuni, Mater. Res. Bull.40, 694 (2005).
- [30] K. Wang, Dong, X. Wang, C. Zhao, X. Qian, et al., Electrochim. Acta 152, 433 (2015).
- [31] X. Ding, L. Qu, R. Yang, Y. Zhou, and J. Li, Luminescence 30, 465 (2015).
- [32] A. S. Emrani, N. M. Danesh, P. Lavaee, M. Ramezani, K. Abnous, et al., Food. Chem. 190, 115 (2016).
- [33] S. Patchkovskii, J. S. Tse, S. N. Yurchenko, L. Zhechkov, T. Heine, et al., PNAS, 102, 10439 (2005).
- [34] J. M. Soler, E. Artacho, J. D. Gale, A. García, J. Junquera, et al., J. Phys. Condens. Matter 14, 2745 (2002).
- [35] N. Troullier, J. L. Martins, Phys. Rev. B 43, 1993 (1991).
- [36] X. Qin, W. Feng, X. Yang, J. Wei, and G. Huang, Sens. Actuators B Chem. 272, 60 (2018).
- [37] H. B. Na, X. F. Zhang, M. Zhang, Z. P. Deng, X. L. Cheng, et al., Sens. Actuators B Chem. 297, 126816 (2019).
- [38] L. M. G. Padua, J. M. Yeh, K. S. Santiago, Polymers 11, 1918
- [39] Z. J. Ke, D. L. Tang, X. Lai, Z. Y. Dai, and Q. Zhang, Optik 157, 1094 (2018).